Mon. Not. R. Astron. Soc. **374,** 150–158 (2007) doi:10.1111/j.1365-2966.2006.11117.x

What is the origin of the soft excess in active galactic nuclei?

Małgorzata A. Sobolewska⋆ and Chris Done⋆
Department of Physics, University of Durham, South Road, Durham DH1 3LE

Accepted 2006 September 28. Received 2006 September 26; in original form 2006 September 5

ABSTRACT

We investigate the nature of the soft excess below 1 keV observed in active galactic nuclei. We use the *XMM–Newton* data of the low-redshift, optically bright quasar, PG 1211+143, and we compare it with the narrow-line Seyfert 1 galaxy, 1H 0707−495, which has one of the strongest soft excesses seen. We test various ideas for the origin of the soft X-ray excess, including a separate spectral component (for example, low-temperature Comptonized emission), a reflection-dominated model, or a complex absorption model. All three can give good fits to the data, and χ^2-fitting criteria are not sufficient to discriminate among them. Instead, we favour the complex absorption model on the grounds that it requires less extreme parameters. In particular, the geometry appears to be more physically plausible as the reflected component in the smeared absorption model is no longer dominant, and relativistic distortions, while still clearly present, are not tremendously larger than expected for a disc around a Schwarzchild black hole.

Key words: accretion, accretion discs – atomic processes – galaxies: active – galaxies: individual: PG 1211+143 – galaxies: individual: 1H 0707−495 – X-rays: galaxies.

1 INTRODUCTION

The X-ray spectra of active galactic nuclei (AGN) and quasars have long been known to often contain a 'soft excess' component at energies below ∼1 keV (e.g. Turner & Pounds 1988). This rises rather smoothly above the extrapolation of the power-law continuum seen in the 2–10 keV band, and seems to connect on to the peak of the UV accretion disc spectrum (Zheng et al. 2001; Czerny et al. 2003). This shape is suggestive of low-temperature, high optical depth Comptonization of the inner accretion disc, in addition to the high-temperature, low optical depth Comptonization required to produce the high-energy power law (e.g. Page et al. 2004a). However, the temperature of this additional component seems remarkably constant in high mass-accretion rate objects ($L/L_{\rm Edd} > 0.1$), despite a large range in black hole mass and hence inferred accretion disc temperature (Czerny et al. 2003; Gierliński & Done 2004, hereafter GD04; Crummy et al. 2006). The nature of this soft excess becomes even more puzzling when compared to the spectra of Galactic black hole (GBH) binary systems. These can indeed show a low-temperature, high optical depth Comptonized component in addition to the disc and high-energy power-law spectrum (in the very high state). However, while it is initially tempting to identify this as the GBH counterpart of the soft excess seen in AGN (Page et al. 2004b; Murashima et al. 2005), the parameters required are rather different, most obviously in the fact that the temperature of this component is *variable* in the GBH (Kubota, Makishima & Ebisawa 2001; Kubota & Done 2004).

AGN with the largest soft excesses, generally narrow-line Seyfert 1 galaxies (NLS1; Boroson 2002), also often show a strong deficit at ∼7 keV which again has no obvious identification (Boller et al. 2002; Fabian et al. 2002, 2004, 2005; Tanaka, Boller & Gallo 2005). These objects are often highly luminous, close to the Eddington limit, yet their underlying high-energy 2–10 keV spectrum can appear to be rather hard (e.g. GD04; Crummy et al. 2006). All Galactic black holes at $L/L_{\rm Edd} \sim 0.5$–1 have intrinsically soft power law Comptonized emission (e.g. Remillard & McClintock 2006), though occasional super-Eddington source spectra can be harder (e.g. V404 Cyg: Życki, Done & Smith 1999).

The constancy of temperature for the soft excess emission could plausibly point to an origin in atomic processes. In particular, there is an abrupt increase in opacity in partially ionized material between ∼0.7 and 3 keV due to O VII/O VIII and Fe L transitions which can produce a large increase in reflected or transmitted flux below 0.7 keV, making the apparent soft X-ray excess. The corresponding rise in reflected or transmitted flux above 2–3 keV could also artificially harden the high-energy spectrum, while the same material might also have strong iron features, giving a simultaneous explanation of the 7-keV deficit.

By contrast, models where the soft excess is a separate continuum component require some other explanation for the origin of the iron features and hard spectra, such as partial covering of the source by cold absorbing material (Boller et al. 2002; Tanaka et al. 2004). However, the neutral iron edge at 7.1 keV in these models is not big enough to fit the strongest observed features unless iron

⋆E-mail: m.a.sobolewska@durham.ac.uk (MAS); chris.done@durham.ac.uk (CD)

is very overabundant, at least five to seven times the solar value (Gallo et al. 2004; Tanaka et al. 2004; Gallo 2006). More generally, such models seem contrived as the iron features and hard spectra appear to be correlated with the soft excess, pointing to a common origin for the hard and soft spectral complexity (Boller et al. 2003; Reeves, Porquet & Turner 2004; Tanaka et al. 2005). This connection is strongly supported by spectral variability. The rms spectra from these objects typically show more variability in the 0.7–3 keV range than at higher or lower energies (e.g. Gallo et al. 2004; Ponti et al. 2004, 2006). The spectrum below 0.7 keV, which is dominated by the soft excess, typically has the same variability as the spectrum above 3 keV, showing that they are almost certainly linked to the same component. The amplified variability in the 0.7–3 keV region is compelling evidence for an atomic origin for the spectral complexity, as it is exactly over this energy range that the atomic features dominate (Gierliński & Done 2006), but both reflection and absorption can match the variability spectra seen (Gierliński & Done 2006; Ponti et al. 2006).

One obvious problem with the atomic models is that they predict strong, sharp atomic features from the partially ionized material. Such characteristic narrow absorption lines and sharp edges are seen in AGN (warm absorbers) but these can be easily isolated using high spectral resolution data (see e.g. Blustin et al. 2005 and references therein), and a strong *smooth* soft excess remains. Large velocity smearing is the only way to keep an atomic origin of the soft excess. If at least some of the material is moving at moderately relativistic speeds, the characteristic line/edge features become strongly broadened into a quasi-continuum. Such speeds naturally arise only close to the black hole, so the atomic models predict that the soft excess is formed in regions of strong gravity, irrespective of whether it arises from partially ionized reflection or absorption. However, it is important to distinguish between a reflection or absorption origin for the soft excess, as they give very different geometries and have different implications for our understanding of the X-ray source. In reflection, the partially ionized material is optically thick and out of our line of sight. The accretion disc is the obvious identification but in order to produce the strongest soft excesses a reflection model requires that the intrinsic continuum is strongly suppressed, perhaps by the disc fragmenting or by extreme lightbending (Fabian et al. 2002, 2004, 2005; Miniutti & Fabian 2004). The velocity structure should be Keplerian, and the large inferred smearing implies a very small inner disc radius, and hence extreme Kerr space–time and/or extremely centrally concentrated emissivity (e.g. Miniutti & Fabian 2004). By contrast, in an absorption origin, the partially ionized material is optically thin, and seen in our line of sight. This implies that it is some sort of wind from the disc, so its velocity structure is not well defined, and cannot easily give constraints on the space–time (GD04; Chevallier et al. 2006; Schurch & Done 2006).

The structure of this paper is as follows. In Section 2, we try to distinguish between the reflection and absorption models for the soft excess. We calculate the strength of the soft excess in both models, showing that the largest observed soft excesses can be produced in the absorption model by simply changing the column of material in the line of sight. In Section 3 we explicitly compare reflection and absorption models by fitting data from PG 1211+143 and 1H 0707−495, representative of the largest soft excesses seen in quasars and NLS1s, respectively. Both models give comparably good fits to the data in terms of χ^2 criteria, as does the more phenomenological model of a separate soft component. Statistics cannot discriminate between them, and depending on χ^2 alone may be somewhat misleading as there are systematic uncertainties in the models (such as range of ionization states present) which probably dominate the residuals.

How then can we distinguish between them? The *XMM–Newton* data is fairly high signal-to-noise ratio, moderate spectral resolution and fairly broad bandpass (0.3–10 keV), yet neither energy nor variability spectra can clearly discriminate between these models. In Section 4, we suggest that simultaneous data at higher energies may be able to break these spectral model degeneracies. We also review the physical plausibility of the models, which leads us to favour the smeared absorption as the origin of the soft excess.

2 COMPARISON OF REFLECTION AND ABSORPTION MODELS FOR THE SOFT EXCESS

We use the results of GD04 to determine the range of soft excess strengths which are required by the data. They defined $R_{\rm x}$ as the ratio of unabsorbed 0.3–2 keV fluxes in the soft excess and power-law continuum components, respectively. However, the data need to be fitted in order to use such parametrization. An alternative measure of the size of soft X-ray excess, which does not require spectral fitting, is to assume that the spectrum is a power law with single photon index Γ but with a step in normalization at 0.7 keV, i.e. $f(E) = AE^{-\Gamma+1}$ for $E \geqslant 0.7$ keV, and $f(E) = SAE^{-\Gamma+1}$ for $E < 0.7$ keV. The ratio S of the spectrum at soft energies to that expected from an extrapolation of the higher energy power law is often plotted in the literature (e.g. Porquet et al. 2004), and relates rather simply to the soft excess parametrization of GD04 by $R_{\rm x} = a(\Gamma)(S - 1) + 1$ where $a(\Gamma) = (0.7^{2-\Gamma} - 0.3^{2-\Gamma})/(2^{2-\Gamma} - 0.3^{2-\Gamma}) = 0.3$–$0.6$ for $\Gamma = 1.5$–2.5. Thus with this parametrization we can use the objects with ratio plots in the literature as well as data from the sample of GD04. These range from 2 to 3 for the majority of the PG quasars (GD04; Porquet et al. 2004) to $\gtrsim$10 for some NLS1s (Boller et al. 2002, 2003; Reeves et al. 2004).

In reflection models, the size of the soft X-ray excess will be set by the solid angle subtended by the reflecting material, and its ionization state. We use ionized reflection spectra of Ross & Fabian (2005) publicly available as ATABLE models in XSPEC. We fix the inclination at 30°, and smear the model by relativistic effects so that the line features do not dominate (we fix the reflector emissivity at 3, and its inner and outer radius at $1.24R_{\rm g}$, i.e. extreme Kerr, and $400R_{\rm g}$, respectively).

Fig. 1(a) shows how the spectral ratio S (evaluated at 0.5 keV) depends on the ionization parameter of the reflector for the maximum 'normal' reflection amount of $\Omega/2\pi = 1$. First, it is apparent that partial ionization is required in order to have the soft excess. The strong jump in opacity due to the transition from the oxygen K and iron L shell is only present when these species are present, which requires ($2.5 \leqslant \log\ \xi \leqslant 3.5$). Secondly, the strength of this soft excess is rather limited. Allowing for super solar iron abundance does not change this conclusion (see Fig. 1a) as it is set by the solid angle of the reflector. Even in the limit of perfectly ionized reflection below 0.7 keV and no reflection at 3 keV, this sets a maximum $S \sim 1 + \Omega/2\pi < 2$ for 'normal' reflected emission with $\Omega/2\pi < 1$.

The majority of soft excesses seen from the PG quasars do indeed have $S \lesssim 2$–3 (GD04; Porquet et al. 2004), but the largest soft excesses seen require that the spectrum is dominated by the reflected emission rather than the intrinsic continuum (Fig. 1b). This could be done in a geometry in which the disc fragments, or from lightbending distorting the illumination pattern of an initially isotropic source (Fabian et al. 2002, 2004; Miniutti & Fabian 2004). However, if the lightbending interpretation is correct, this predicts a correlation

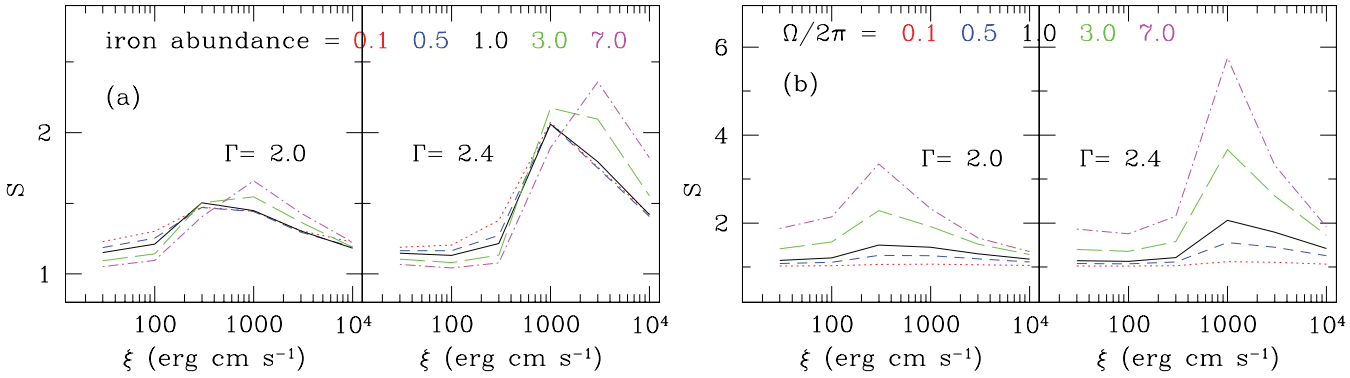

Figure 1. Strength of the soft excess in a reflection model (with a photon index of underlying continuum of $\Gamma = 2.0$ and 2.4) as a function of ionization parameter and (a) iron abundance for $\Omega/2\pi = 1$, (b) amplitude of reflection for solar abundance. The curves correspond to Fe abundance (or $\Omega/2\pi$) of 0.1 (dotted curve), 0.5 (short-dashed curve), 1 (solid curve), 3 (long-dashed curve) and 7 (dot–dashed curve).

between the solid angle (reflection dominance of the spectrum) and the amount of smearing as stronger lightbending also focuses the illumination more strongly on to the inner disc. Such a correlation is not seen in the data (Crummy et al. 2006).

Absorption models also require a range of ionization parameter as again they are dependent on the strong opacity jump produced by oxygen K/iron L transitions. To quantify the soft excess strength in the smeared absorption model we assume that the absorber has a Gaussian velocity distribution with $\sigma = 0.2c$ modifying an intrinsic power-law continuum with photon index of $\Gamma = 2$. The soft excess is then defined as the ratio of the absorption model to extrapolation of a power-law fit to the 3–8 keV spectrum at 0.5 keV, and its strength as a function of ionization parameter is shown in Fig. 2. The soft excess disappears for log $\xi \lesssim 2$ as the neutral material absorbs all the soft X-ray emission, and for log $\xi \gtrsim 4$ where the column is completely ionized and transparent at all energies. However, the soft excess at log $\xi \sim 3$ is now strong enough to match the largest seen. (Note the increase in y-axis range of this figure compared to the reflection plots, and the log scale.) Changing the column changes the size of soft excess, as shown in Fig. 2.

Both the reflection and absorption models require a 'fine-tuned' ionization parameter, such that oxygen is partially ionized. This may be explained in the absorption models by the ionization instability,

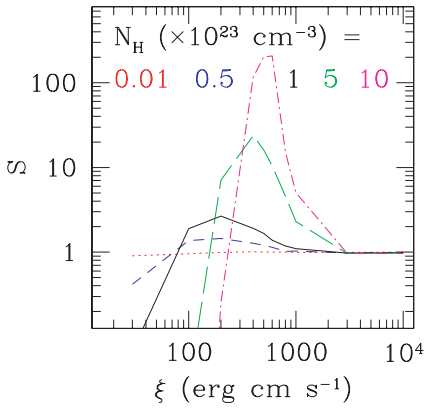

Figure 2. Strength of the soft excess in an absorption model as a function of ionization parameter for column densities N_H ($\times 10^{23}$ cm^{-3}) of 0.01 (dotted curve), 0.5 (short-dashed curve), 1 (solid curve), 5 (long-dashed curve) and 10 (dot–dashed curve). The sharp absorption features were smeared with $\sigma = 0.2$. In this model, the strength of the soft excess does not depend on the photon index of the continuum.

which results from X-ray illumination of material in some sort of pressure balance (Chevallier et al. 2006). However, there is no obvious way to do this in reflection models. The ionization instability in a disc *reduces* the extent of the partially ionized zone (Nayakshin, Kazanas & Kallman 1999), yet to produce a soft excess from reflection requires that the partially ionized zone has to dominate over the entire photosphere of the disc. It is very difficult for a hydrostatic disc to produce the soft excess (Done & Nayakshin, in preparation). Even without the response of the disc to the irradiating flux, X-ray illumination of a standard Shakura–Sunyaev disc gives an ionization parameter

$$\xi(r) = \frac{L_X}{n(r)(H^2 + R^2)} = 2 \times 10^{11}\, f\, \dot{m}^3\, \alpha\, r^{-1.5}\, (h^2 + r^2)^{-1}\, c_3^{-1}\ \mathrm{erg\,cm\,s^{-1}},$$

where disc density $n(r) = 2.4{\times}10^7 \alpha^{-1} \dot{m}^{-2} m_9^{-1} r^{1.5} c_3$ cm^{-3} is taken from Laor & Netzer (1989), α is the viscosity parameter, $\dot{m} = L/L_{\rm Edd}$, $L_{\rm Edd} = 1.3{\times}10^{47} m_9$ ergs s^{-1}, $m_9 = M/(10^9\ \mathrm{M}_\odot)$, $L_X = fL$, so that f is the fraction of the luminosity which goes into hard X-rays, c_3 is a relativistic correction, and all the distances are expressed in terms of gravitational radius, $R_g = 1.5 \times 10^{14}\, m_9$, i.e. $R = rR_g$, $H = hR_g$. A similar relation is given by Ross & Fabian (1993). This can give the required value of $\xi \sim 10^{2-3}$ erg cm s^{-1}, but is very dependent on the parameters, changing particularly rapidly with $\dot{m}$. An alternative prescription for the viscosity, where the heating goes as the geometric mean of the gas and radiation pressure (which may be more physically realistic: Merloni 2003), results in a denser disc and hence a lower ionization parameter of

$$\xi(r) = 8 \times 10^6\, f\, \dot{m}^{2.11} m_9^{-0.12}\, \alpha^{0.88}\, (h^2 + r^2)^{-1}\, r^{-0.33}\, c_7^{-1}\ \mathrm{erg\,cm\,s^{-1}},$$

where c_7 is a relativistic correction. This is less strongly dependent on parameters, but both require some method of 'fine-tuning' the source height relative to $\dot{m}$ in order to produce the observed narrow range in ionization parameter.

3 SPECTRAL FITTING

The theoretical considerations in the previous section favour an absorption origin for the soft excess as it can reproduce the observed range of soft excess strengths without extreme geometries, and the required 'fine-tuning' of the ionization parameter may have an explanation in terms of ionization instability. However, given the model uncertainties, observations may be a better way to distinguish between reflection and absorption as the origin of the soft excess.

We use *XMM–Newton* data from two representative objects with large soft excesses, the low-redshift ($z = 0.085$) quasar, PG 1211+143, and the NLS1 galaxy 1H 0707−495 ($z = 0.0411$). PG 1211+143 is one of the extensively studied objects from Palomar-Green Bright Quasars Survey and was selected based on its optical brightness suggesting super-Eddington accretion rate (Boroson 2002, GD04). 1H 0707−495 is less luminous than PG 1211−143, but it shows one of the strongest soft excesses seen. Both objects show a drop of the flux at 7 keV, which is especially dramatic in the case of 1H 0707−495 (Boller et al. 2002). Their spectra are accretion disc dominated which suggests that they are counterparts of X-ray binaries in the high/soft state (Janiuk, Czerny & Madejski 2001).

We use the Epic PN data, extracted from the data base using standard techniques (see GD04). We fit these data in the 0.3–10 keV energy band using XSPEC to explicitly compare the models for the soft excess.

First, we set up a baseline model where the soft excess is a separate component. We use the COMPTT code of Titarchuk (1994) to describe the soft excess as Comptonization of disc photons (assumed to be at fixed $T_{\rm bb} = 10$ eV) on electrons of temperature $kT_{\rm e}$, and the optical depth, τ (Model 1). The soft excess shape generally cannot easily constrain these two parameters separately, so we fixed $\tau = 50$. The hard X-ray tail was modelled by a power law (with photon index Γ and normalization) together with its reflection from the accretion disc. We use the publicly available models of Ballantyne, Iwasawa & Fabian (2001), which were then relativistically smeared using the Laor (1991) kernel. This reflection is characterized by the ionization parameter of the reflecting matter, ξ, and its normalization, while the smearing parameters are the inner and outer radii of the reflecting disc, together with its inclination (fixed at 30°). We fix the emissivity at 3, which results in rather small value of the outer radius of the reflector. Conversely, fixing the outer radius at (say) $400R_{\rm g}$ would result in an emissivity greater than 3.

This baseline model is then modified to describe different potential origins for the soft excess. In a reflection origin (Model 2) we replace the COMPTT component (which had two free parameters, namely electron temperature and normalization) with another relativistically smeared reflector (four additional parameters: ionization, normalization, inner and outer radii), while in Model 3 we replace it with the relativistically smeared absorption (the SWIND model of Gierliński & Done 2006[1] which has three additional parameters: ionization, column and Gaussian velocity smearing, σ).

All models were additionally modified by the cold Galactic absorption (the WABS model with column densities fixed at 2.7×10^{20} and 5.8×10^{20} cm^{-2} for PG 1211+143 and 1H 0707−459, respectively), cold absorption at the redshift of the source (the ZWABS model with $z = 0.085$ and 0.0411 for PG 1211+143 and 1H 0707−459, respectively) and warm absorption accounting for the narrow features in the spectra, modelled with the XSTAR code (Bautista & Kallman 2001). We use the most recent XSTAR table models which are publicly available (grid 25) computed for turbulent velocity of 200 km s^{-1} and valid for wide range of ionization parameter and column density ($1 < \log\ \xi < 5$, $21 < \log\ N_{\rm H} < 24$). Hence, the only thing that differentiates the models is the description of the origin of the soft excess.

The spectral decomposition implied by each model is shown in Figs 3 and 4 for PG 1211+143 and 1H 0707−459, respectively. The high-resolution data have been rebinned for clarity of the plots. The detailed model parameters are given in Tables 1–4. These show that the soft excess, if described by Model 1, originates in the Comptonization of disc photons on electron plasma with temperature of $kT_{\rm e} \simeq 0.12$–0.14 keV. The power-law modelling the high-energy part of the spectrum is relatively hard, $\Gamma \simeq 1.8$–2, and it is reflected by an ionized material with $\log\ \xi \simeq 2.6$–3.0, in the innermost parts of the accretion flow (at 5–$9R_{\rm g}$ and 3–$7R_{\rm g}$ for PG 1211+143 and 1H 0707−495, respectively). The last stable circular orbit in the Schwarzschild metric around a non-rotating black hole is located at $6R_{\rm g}$, so neither of these significantly requires a rotating Kerr black hole, though the correspondingly small outer radii indicate that the emissivity is highly centrally concentrated in both AGN. The amount of reflection as compared to the intrinsic power-law emission implies a solid angle of $\Omega/2\pi \sim 4$ for PG 1211+143. For 1H 0707−459 the best fit has no intrinsic power-law emission, so that the high-energy spectrum is formed solely by reflection. In both AGN the reflection is partially ionized, so that around half of the soft excess is made by the reflected component. However, this single reflector alone cannot describe the shape of the spectrum; χ^2 increases by 56 (940 d.o.f. in the model with COMPTT) and 175 (286 d.o.f in the model with COMPTT) in PG 1211+143 and 1H 0707−495, respectively, if the Comptonization component is removed.

However, if instead of the COMPTT component, another smeared reflector is introduced (Model 2) then the soft excess can be well fit by the combination of the two reflectors with different ionization states, one mostly neutral (with $\log\ \xi < 2$) and the other highly ionized (with $\log\ \xi \simeq 3$–4). However, this leaves systematic residuals around ∼7 keV. A better fit to 1H 0707−495 was obtained by assuming that the iron abundance in both reflectors was twice the solar value ($\Delta\chi^2 = 18$ for 284 d.o.f.). The improvement was mainly due to the reduction in residua around the iron feature. In PG 1211+143, the fits with the solar and twice the solar iron abundances are of the same quality. Substantial relativistic smearing (in the case of PG 1211+143 requiring an extreme Kerr black hole) is required to model the data. The incident X-ray radiation has a moderate photon index in PG 1211+143 ($\Gamma \simeq 2.1$) and is rather soft in 1H 0707−495 ($\Gamma \simeq 2.6$) but is not seen in either AGN. The best-fitting spectra are dominated by the two reflectors only, implying a geometry in which the intrinsic power-law emission is strongly suppressed, so it makes a negligible contribution to the observed radiation.

Replacing the second reflector with smeared absorption gives rather different results (Model 3). The remaining reflector subtends a solid angle $\Omega/2\pi < 2$, much smaller than in the case of reflection-dominated model. It is partially ionized with $\log\ \xi \simeq 2.5$, and fairly close to the black hole (5–$12R_{\rm g}$ and $\sim 30R_{\rm g}$ for PG 1211+143 and 1H 0707−495, respectively) but is not so strongly smeared as to give constraints on spin. The partially ionized reflection does contribute to the soft excess (see also Chevallier et al. 2006), though this component could also be produced by emission from the smeared absorbing material (Schurch & Done 2006). This latter has ionization parameter $\log\ \xi = 2.4$–2.9, high column density, $N_{\rm H} \simeq (5$–$40) \times 10^{22}$ cm^{-2} and large velocity shear ($\sigma = v/c \simeq 0.1$ and 0.4 for PG 1211+143 and 1H 0707−495, respectively). Such matter may be physically pictured as some sort of accretion disc wind, which may be differentially rotating as well as accelerating (and/or decelerating) radially. The assumed Gaussian velocity dispersion is only a zeroth-order approximation to this complexity.

While the reflection model leaves some systematic residuals around the iron line, these are much more prominent in the absorption model. Especially for 1H 0707−495, the absorption model does not describe the sharp drop around 7 keV in the spectrum. This is partially due to the assumption of Gaussian velocity smearing

[1] SWIND model is available from http://heasare.gsfc.nasa.gov/docs/xanadu/xspec/models/swind1.html

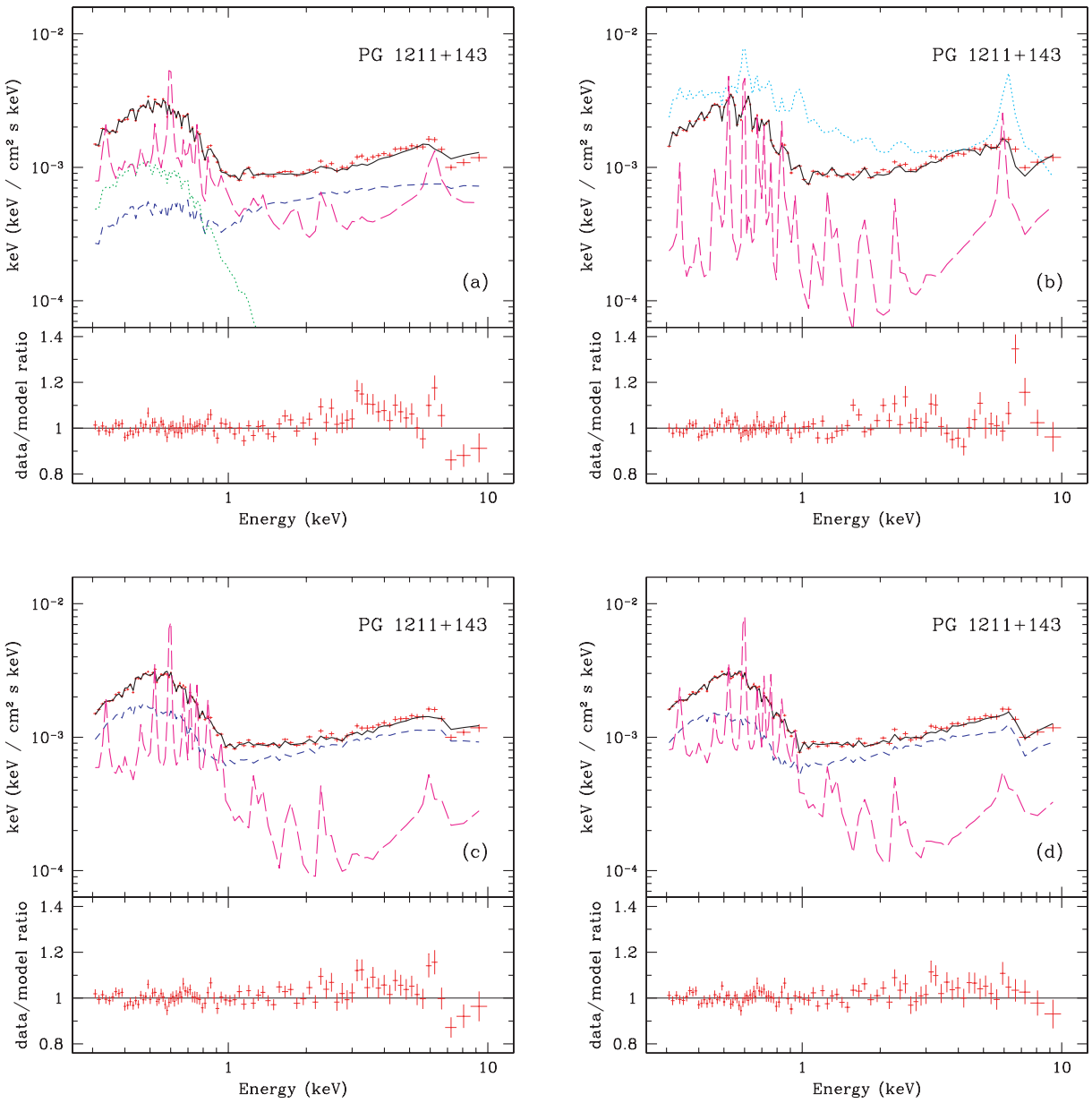

Figure 3. Modelling the soft excess in PG 1211+143. Solid curve: the best-fitting spectra. (a) Model 1 – a low-temperature Comptonization (green/dotted curve), power law (blue/short-dashed curve) and ionized reflection (magenta/long-dashed curve). (b) Model 2 – two reflectors (magenta/dotted and cyan/long-dashed curves) with different column densities and ionization states, located at different radii. (c) Model 3 – a power law (blue/short-dashed curve) subject to relativistically smeared absorption and reflection (magenta/long dashed). (d) Model 4 – same as Model 3 but with the intrinsic power law modified by the addition of a line with P Cygni profile modelling the iron feature. All four models are additionally affected by Galactic absorption, cold absorption at the redshift of the sources and two warm absorbers (see the text).

in the absorption model. By definition this cannot produce sharp features. None the less, sharp features can be produced by a wind with strong velocity shear. P Cygni profiles are an obvious example of this. Done et al. (2006) show that the 7-keV feature in these data from 1H 0707−495 can be fit using a P Cygni profile from emission/absorption/scattering of the He- or H-like resonance iron Kα line at 6.7 or 7.0 keV, respectively. We extend the smeared absorption model by including a P Cygni profile to model the ∼7 keV feature (Model 4: two additional free parameters being the absorption optical depth of the line and its rest energy). Thus, the incident power law is not only affected by the smeared absorption but also has a P Cygni line as in Done et al. (2006).

In Model 4 applying the P Cygni profile to the ∼7 keV feature results in a much improved fit around the iron feature. The inferred line rest-frame line energy of 6.85–7.14 keV, which is consistent with either He- or H-like iron. The fits give $v_\infty/c = 0.5_{-0.2}$ and $0.5_{-0.1}$ for PG 1211+143 and 1H 0707−495, correspondingly. The resonance absorption line optical depth in PG 1211+143 is relatively low, $\tau = 0.23^{+0.19}_{-0.09}$, and in 1H 0707−495 it is higher and yields $\tau = 2.0^{+4.0}_{-1.1}$. As in Model 3, the parameters of the remaining reflector are much less extreme than for the reflection model of the soft excess (Model 2). In fact, the deconvolved spectra in Figs 3(d) and 4(d) show that this reflector contributes mainly to producing soft X-ray lines rather than the iron feature, indicating that the reflection

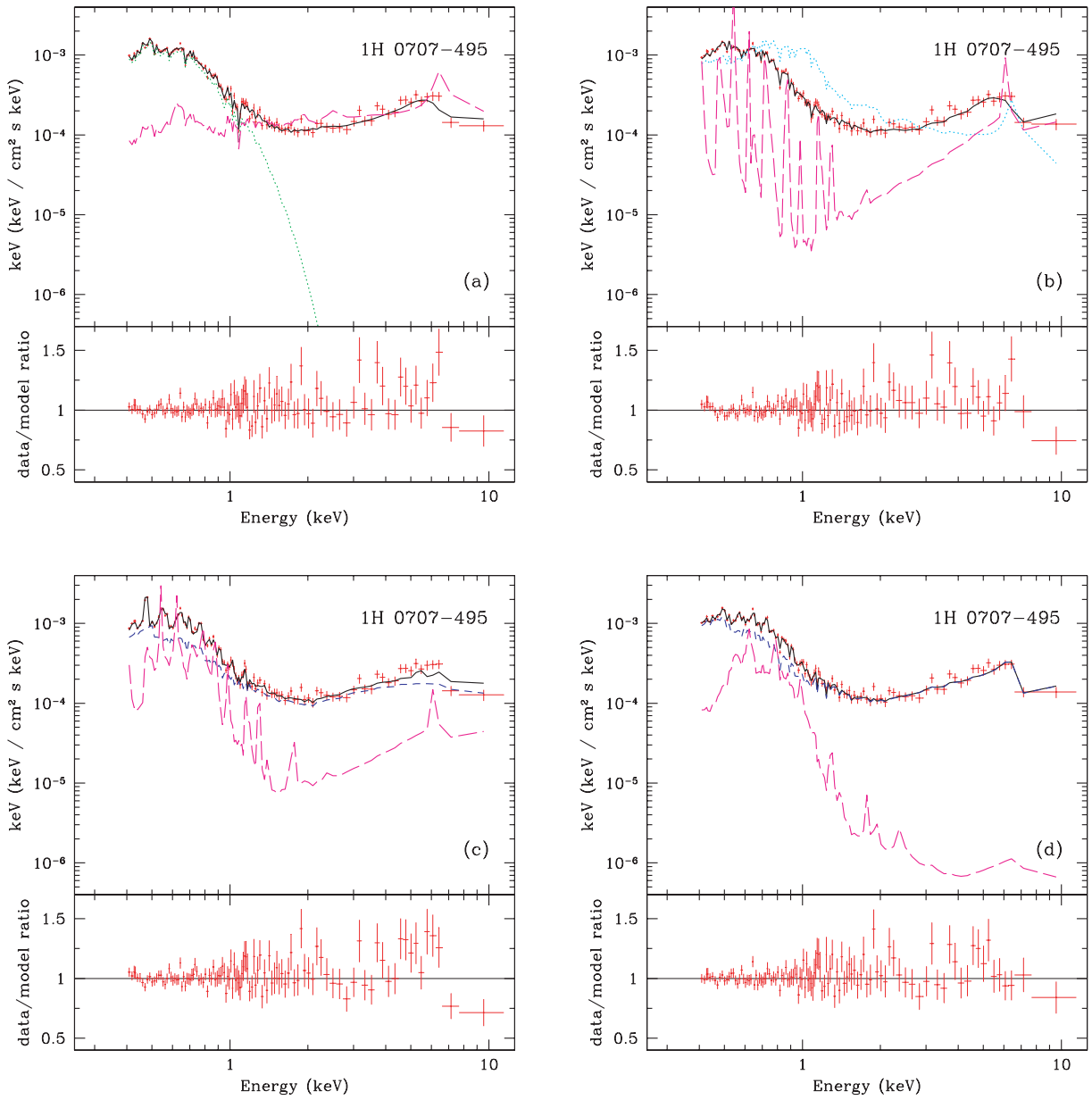

Figure 4. Modelling the soft excess in 1H 0707−495. (a), (b), (c) and (d) as in Fig. 3. (a) Model 1 in 1H 0707−495 does not require intrinsic power law.

Table 1. Best-fitting parameters of Model 1 to PG 1211+143 and 1H 0707−495 data. Plasma optical depth was fixed at $\tau = 50$, emissivity at 3 and inclination at 30°. No intrinsic power-law emission is seen in the model for 1H 0707−495.

	kT_e (keV)	Γ	log ξ	R_i R_g	R_f R_g	$\Omega/2\pi$
PG	0.136 ± 0.003	$2.02^{+0.03}_{-0.02}$	$2.58^{+0.04}_{-0.01}$	$4.5^{+0.7}_{-0.5}$	$8.7^{+1.8}_{-2.2}$	4.12 ± 0.49
1H	0.122 ± 0.002	$1.81^{+0.07}_{-0.09}$	$3.00^{+0.02}_{-0.15}$	$3.0^{+1.0}_{-0.5}$	$7.4^{+4.5}_{-1.8}$	∞

parameters may be further distorted if there is also emission from the wind (see e.g. Schurch & Done 2006).

Table 5 contains parameters of the warm absorbers modifying the continua such as column density, logarithm of the ionization parameter and redshift of the warm absorbers. We find that including the second warm absorber significantly improves the fits in all cases. The last column in Table 5 contains the column density of the cold absorption at the redshifts of the source. It is comparable with the Galactic cold absorption for all models except Model 2 and Model 4 (the 1H 0707−495 case) for which only the upper limit can be given.

The best-fitting values of χ^2 and number of degrees of freedom are given in Table 6. In PG 1211+143, the worst fit is obtained with the reflection-dominated model. The smeared absorption model is statistically significantly better than the model with low-temperature Comptonization (F-test probability of chance improvement 5×10^{-8}). Modelling the iron feature with a P Cygni profile further improves the fit (F-test probability 10^{-5}). In 1H 0707−495, the smeared absorption model fits worse than either reflection-dominated model or the model with additional

Table 2. Best-fitting parameters of Model 2 to PG 1211+143 and 1H 0707−495 data. Missing upper (lower) limit indicates that the parameter reached its upper (lower) boundary allowed in the fit. Emissivity was fixed at 3 and inclination at 30° and the iron abundance was twice the solar value. The fits are reflection dominated, so $\Omega/2\pi = \infty$.

	Γ	log ξ_1	R_{i_1} R_g	R_{f_1} R_g	log ξ_2	R_{i_2} R_g	R_{f_2} R_g
PG	$2.127^{+0.006}_{-0.005}$	3.13 ± 0.01	$1.31^{+0.21}_{-0.07*}$	$3.20^{+0.10}_{-0.06}$	1.88 ± 0.02	22^{+3}_{-8}	33^{+8}_{-4}
1H	$2.592^{+0.009}_{-0.013}$	$4.00_{-0.04}$	3.4 ± 0.7	$4.4^{+1.4}_{-1.5}$	$1.5^{+0.2}$	$1.89^{+0.44}_{-0.65*}$	20^{+16}_{-8}

Table 3. Best-fitting parameters of Model 3 to PG 1211+143 and 1H 0707−495 data. An asterisk indicates that the upper (lower) limit allowed was reached with $\Delta\chi^2 < 2.71$. Emissivity was fixed at 3 and inclination at 30°.

	Γ	N_H ($\times 10^{22}$ cm^{-2})	log ξ_a	σ	log ξ_r	R_i R_g	R_f R_g	$\Omega/2\pi$
PG	$2.34^{+0.03}_{-0.05}$	$5.3^{+0.8}_{-0.6}$	$2.43^{+0.04}_{-0.06}$	0.10 ± 0.01	$2.48^{+0.04}_{-0.07}$	4.8 ± 0.7	12^{+6}_{-3}	1.67 ± 0.47
1H	$2.994^{+0.006*}_{-0.034}$	41^{+9}_{-13}	$2.89^{+0.06}_{-0.08}$	$0.36^{+0.09}_{-0.07}$	2.478 ± 0.001	$32.4^{+0.3}_{-2.0}$	33.8 ± 0.5	1.59 ± 0.83

Table 4. Best-fitting parameters of Model 4 to PG 1211+143 and 1H 0707−495 data. An asterisk indicates that the upper (lower) limit allowed was reached with $\Delta\chi^2 < 2.71$. Emissivity was fixed at 3 and inclination at 30°.

	Γ	N_H ($\times 10^{22}$ cm^{-2})	log ξ_a	σ	E (keV)	v_∞/c	τ	log ξ_r R_g	R_i R_g	R_f	$\Omega/2\pi$
PG	$2.29^{+0.07}_{-0.05}$	$5.0^{+1.1}_{-0.6}$	$2.43^{+0.06}_{-0.05}$	0.09 ± 0.01	$6.58^{+0.08}_{-0.10}$	$0.5_{-0.2}$	$0.23^{+0.19}_{-0.09}$	$2.49^{+0.04}_{-0.13}$	$4.4^{+0.7}_{-0.6}$	12^{+6}_{-2}	1.95 ± 0.65
1H	$2.90^{+0.07}_{-0.19}$	48^{+2*}_{-11}	$2.93^{+0.05}_{-0.19}$	$0.43^{+0.07*}_{-0.06}$	6.58 ± 0.17	$0.5_{-0.1}$	$2.0^{+4.0}_{-1.1}$	$3.12^{+0.15}_{-0.08}$	60^{+5}_{-11}	66^{+5}_{-2}	0.011 ± 0.002

Table 5. Best-fitting parameters for warm absorbers (with $v_{\rm turb} = 200$ km s^{-1}) and cold absorption at the redshift of PG 1211+143 and 1H 0707−495. Missing upper (lower) limit indicates that the parameter reached its upper (lower) boundary allowed in the fit. An asterisk indicates that the upper (lower) limit allowed was reached with $\Delta\chi^2 < 2.71$. Emissivity was fixed at 3 and inclination at 30°.

	N_{H_1} (cm^{-2})	log ξ_1	z_1	N_{H_2} (cm^{-2})	log ξ_2	z_2	N_{H_z} (cm^{-2})
				PG			
Model 1	$(5.3 \pm 0.4)\times 10^{21}$	$1.57^{+0.03}_{-0.04}$	$-0.015^{+0.001}_{-0.002}$	$3.2^{+1.5}_{-0.6} \times 10^{22}$	2.79 ± 0.03	$-0.087^{+0.004}_{-0.001}$	$6.6^{+3.7}_{-2.7} \times 10^{19}$
Model 2	$(4.6 \pm 0.3)\times 10^{21}$	$1.65^{+0.03}_{-0.07}$	$0.023^{+0.003}_{-0.005}$	$(1.7 \pm 0.3)\times 10^{23}$	$3.24^{+0.09}_{-0.05}$	$-0.047^{+0.003}_{-0.002}$	$< 2.1 \times 10^{19}$
Model 3	$5.7^{+3.0}_{-2.3} \times 10^{22}$	2.90 ± 0.04	$-0.148^{+0.003}_{-0.002*}$	$1.4^{+0.5}_{-0.3} \times 10^{23}$	$2.89^{+0.07}_{-0.04}$	$-0.059^{+0.003}_{-0.002}$	$1.8^{+0.6}_{-1.1} \times 10^{20}$
Model 4	$4.4^{+4.9}_{-1.9} \times 10^{22}$	2.82 ± 0.04	$-0.065^{+0.007}_{-0.011}$	$5.9^{+4.6}_{-2.0} \times 10^{22}$	$2.84^{+0.05}_{-0.04}$	$-0.150^{+0.002}$	$1.1^{+0.8}_{-0.5} \times 10^{20}$
				1H			
Model 1	$1.5^{+2.4}_{-0.5*} \times 10^{21}$	$1.1^{+0.4}_{-0.1*}$	-0.02 ± 0.04	$9.4^{+1.5}_{-1.9} \times 10^{21}$	$1.73^{+0.07}_{-0.05}$	$-0.148^{+0.006}_{-0.002*}$	$(4.4^{+1.4}_{-1.5})\times 10^{20}$
Model 2	$4.8^{+1.5}_{-1.3} \times 10^{21}$	1.5 ± 0.1	-0.02 ± 0.02	$1.0_{-0.7} \times 10^{24}$	$3.42^{+0.24}_{-0.05}$	$-0.06^{+0.01}_{-0.02}$	$< 1.6 \times 10^{20}$
Model 3	$2.0^{+1.8}_{-1.0*} \times 10^{21}$	$1.5^{+0.4}_{-0.5}$	$-0.02^{+0.02}_{-0.03}$	$3.6^{+6.4*}_{-2.7} \times 10^{23}$	$3.31^{+0.10}_{-0.06}$	$-0.04^{+0.02}_{-0.01}$	$6.3^{+1.1}_{-0.7} \times 10^{20}$
Model 4	$4.0^{+1.5}_{-2.4} \times 10^{21}$	$1.5^{+0.1}_{-0.5*}$	$-0.02^{+0.02}_{-0.03}$	$4.7^{+1.1}_{-0.9} \times 10^{23}$	$3.20^{+0.08}_{-0.07}$	$-0.05^{+0.02}_{-0.01}$	$< 5.9 \times 10^{20}$

Table 6. The χ^2 values and degrees of freedom in spectral fits to the PG 1211+143 and 1H 0707−495 data.

	Model 1	Model 2 χ^2 (d.o.f.)	Model 3	Model 4
PG	994 (940)	1012 (939)	963 (939)	937 (936)
1H	296 (286)	291 (284)	314 (284)	271 (281)

Comptonization. However, including the P Cygni line in a fit improves it dramatically, giving the best overall fit. The F-test probability of chance improvement in Model 4 as compared to Models 1 and 2 is of the order of 10^{-4}.

However, χ^2 criterion alone cannot uniquely distinguish between the three kinds of models as there are many *model* uncertainties that can contribute to χ^2, e.g. in both the reflection and absorption scenarios we expect an (unknown!) range of ionization states to be present. Hence, direct comparison of χ^2 can be misleading when the models are known to be incomplete. Both reflection and absorption models give adequate fits to the data, and rather subtle changes in goodness of fit are not a reliable guide as to which model best describes the soft excess.

A potential possibility to observationally differentiate between the reflection and absorption models may be measuring the high-energy flux with future missions. Based on the interpolation of the best-fitting models we found that the absorption model predicts the 10–30 keV flux at the level of only 50–60 per cent that of

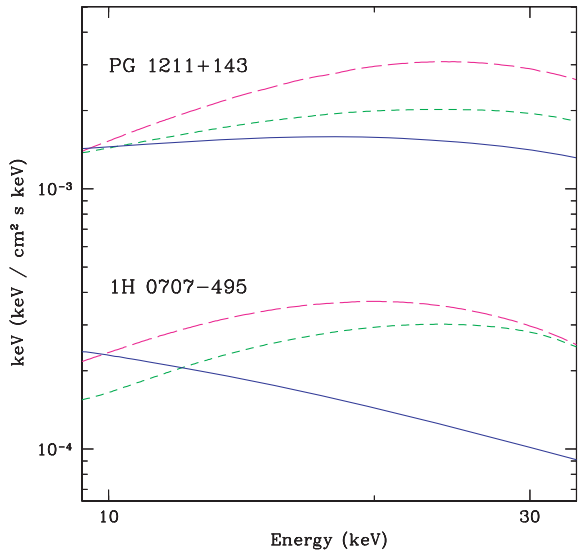

Figure 5. Extrapolation of best-fitting model continua to the 10–30 keV range. The models give different predictions on the 10–30 keV flux, with the reflection-dominated model (magenta/long-dashed curve) producing the highest flux and the smeared absorption model (blue/solid curve) producing the lowest flux. The model with low-temperature Comptonization (green/short-dashed curve) predicts intermediate 10–30 keV flux.

the reflection-dominated model. Fig. 5 shows the predicted model continua (i.e. continua not affected by the warm absorption) in the considered energy band. None the less, we caution that in the most extreme cases, such as that of 1H 0707−495, the inferred wind becomes optically thick to electron scattering (see also Done et al. 2006). The spectrum should then be very messy, with continuum reflection from the wind, as well as absorption and emission from atomic features. This may wash out the expected differences at high energies. Objects with large, rather than extreme, soft excesses (such as PG 1211+143 where the wind is still optically thin) may be better to test its origin.

4 DISCUSSION AND CONCLUSIONS

We tried to determine the origin of the soft excess seen in AGN by fitting 0.3–10 keV *XMM–Newton* spectra of two representative objects with all currently proposed models, namely a separate continuum, reflection and absorption. All these give comparably good fits to the overall continuum given the model uncertainties (such as range of ionization states). Here, we review the physical plausibility of each model to help distinguish between them.

A separate soft excess component involves an emission from an unknown physical process, with unknown 'fine-tuning' mechanism fixing its typical energy. Moreover, this model cannot simultaneously explain the 7-keV feature, nor is it easy to imagine how this can produce the spectral dependence of the variability, where the rms spectra typically peak in 0.7–3 keV band (though it is possible to arrange: Page et al. 2004b). By contrast, both reflection and absorption scenarios are much more plausible, as they give a physical reason for the fixed energy of the soft excess, can reproduce the structure around iron K and give apparently hard spectra in the 2–10 keV band, while the intrinsic spectrum remains soft.

The reflection models can successfully fit the spectra, but the strongest soft excesses require that the intrinsic continuum is suppressed, while the large velocity shear to smear out the atomic features implies extreme spin and/or emissivity (e.g. Crummy et al. 2006).

The alternative absorption model can reproduce the range of observed soft excess strengths by simply changing the column density ($\sim 10^{22-23}$ cm^{-2}), without any requirement for the intrinsic source to be suppressed. Thus, only a quantitative change in column is required, rather than a qualitative change in geometry, as in the case of reflection. Similarly to reflection, a large velocity shear is required in absorption model, but since this is now identified with the wind rather than the disc, it does not directly constrain the space–time or energy extraction process. In pure absorption form, the model does not well fit the most extreme sharp iron features seen at ∼7 keV. However, emission and scattering as well as absorption in a wind can produce a P Cygni profile in He- and H-like iron Kα resonance lines. Including this gives an excellent fit to the feature at 7 keV.

Both reflection and absorption require that the ionization state is 'fine-tuned' such that oxygen is partially ionized. There is no readily apparent reason for this in the reflection models. In fact, the ionization instability may actually give a physical argument against such partially ionized species dominating reflected spectra, making it difficult for a disc in hydrostatic equilibrium to produce any soft excess in reflection (Done & Nayakshin, in preparation). By contrast, this same ionization instability may rather naturally produce the required range of ionization parameter for the absorption model (Chevallier et al. 2006). In addition, on physical grounds we expect strong winds from high $L/L_{\rm Edd}$ accretion discs, especially in AGN featuring a disc flux that peaks in the UV region, where there can be strong line driving (e.g. Proga, Stone & Kallman 2000). The resulting, messy environment appears rather more physically plausible than a clean reflecting disc at high $L/L_{\rm Edd}$, and there is growing evidence for (less extreme) relativistic outflows in the UV spectra of NLS1s (Leighly 2004; Green 2006). Similar material may also be present in GBH binaries at high $L/L_{\rm Edd}$. This might contribute to spectral complexity at energies around iron line, but it is unlikely to produce a soft excess at similar temperatures as in AGN as oxygen is probably always completely ionized due to the much higher accretion disc temperature.

Thus, an absorption origin seems favoured in terms of physical plausibility, though we note that reflection from the disc should also contribute to the spectrum at some level (Chevallier et al. 2006). Higher energy observations soon to be available from *Suzaku* may provide a more sensitive test for objects with the soft excess/iron feature not so large as to require an optically thick wind.

ACKNOWLEDGMENTS

This work is based on observations obtained with *XMM–Newton*, an ESA science mission with instruments and contributions directly funded by ESA Member States and the USA (NASA). This research has made extensive use of NASA's Astrophysics Data System Abstract Service. CD acknowledges financial support through PPARC Senior fellowship. MS and CD thank Marek Gierliński and Nick Schurch for useful discussions.

REFERENCES

Ballantyne D. R., Iwasawa K., Fabian A. C., 2001, MNRAS, 323, 506
Bautista M. A., Kallman T. R., 2001, ApJS, 134, 139
Blustin A. J., Page M. J., Fuerst S. V., Branduardi-Raymont G., Ashton C. E., 2005, A&A, 431, 111
Boller T. et al., 2002, MNRAS, 329, L1

Boller T., Tanaka Y., Fabian A., Brandt W. N., Gallo L., Anabuki N., Haba Y., Vaughan S., 2003, MNRAS, 343, L89
Boroson T. A., 2002, ApJ, 565, 78
Chevallier L., Collin S., Dumont A.-M., Czerny B., Mouchet M., Gonçalves A. C., Goosmann R., 2006, A&A, 449, 493
Crummy J., Fabian A. C., Gallo L., Ross R. R., 2006, MNRAS, 365, 1067
Czerny B., Nikołajuk M., Różańska A., Dumont A.-M., Loska Z., Życki P. T., 2003, A&A, 412, 317
Done C., Sobolewska M., Gierliński M., Schurch N. 2006, MNRAS, in press
Fabian A. C., Ballantyne D. R., Merloni A., Vaughan S., Iwasawa K., Boller T., 2002, MNRAS, 331, L35
Fabian A. C., Miniutti G., Gallo L., Boller T., Tanaka Y., Vaughan S., Ross R. R., 2004, MNRAS, 353, 1071
Fabian A. C., Miniutti G., Iwasawa K., Ross R. R., 2005, MNRAS, 361, 795
Gallo L. C., 2006, MNRAS, 368, 479
Gallo L. C., Boller T., Tanaka Y., Fabian A. C., Brandt W. N., Welsh W. F., Anabuki N., Haba Y., 2004, MNRAS, 347, 269
Gierliński M., Done C., 2004, MNRAS, 349, L7 (GD04)
Gierliński M., Done C., 2006, MNRAS, 371, L16
Green P. J., 2006, ApJ, 644, 733
Janiuk A., Czerny B., Madejski G. M., 2001, ApJ, 557, 408
Kubota A., Done C., 2004, MNRAS, 353, 980
Kubota A., Makishima K., Ebisawa K., 2001, ApJL, 560, L147
Laor A., 1991, ApJ, 376, 90
Laor A., Netzer H., 1989, MNRAS, 238, 897
Leighly K. M., 2004, ApJ, 611, 125
Merloni A., 2003, MNRAS, 341, 1051
Miniutti G., Fabian A. C., 2004, MNRAS, 349, 1435
Murashima M., Kubota A., Makishima K., Kokubun M., Hong S., Negoro H., 2005, PASJ, 57, 279
Nayakshin S., Kazanas D., Kallman T., 1999, Bull. Am. Astron. Soc., 31, 1426
Page K. L., Reeves J. N., O'Brien P. T., Turner M. J. L., Worrall D. M., 2004a, MNRAS, 353, 133
Page K. L., Turner M. J. L., Done C., O'Brien P. T., Reeves J. N., Sembay S., Stuhlinger M., 2004b, MNRAS, 349, 57
Ponti G., Cappi M., Dadina M., Malaguti G., 2004, A&A, 417, 451
Ponti G., Miniutti G., Cappi M., Maraschi L., Fabian A. C., Iwasawa K., 2006, MNRAS, 368, 903
Porquet D., Reeves J. N., O'Brien P., Brinkmann W., 2004, A&A, 422, 85
Proga D., Stone J. M., Kallman T. R., 2000, ApJ, 543, 686
Reeves J. N., Porquet D., Turner T. J., 2004, ApJ, 615, 150
Remillard R. A., McClintock J. E., 2006, ARA&A, 44, 49
Fabian A. C., 2005, MNRAS, 358, 211
Ross R. R., Fabian A. C., 1993, MNRAS, 261, 74
Schurch N. J., Done C., 2006, MNRAS, 371, 81
Shakura N. I., Sunyaev R. A., 1973, A&A, 24, 337
Tanaka Y., Boller T., Gallo L., 2005, in Merloni A., Nayakshin S., Sunyaev R. A., eds, ESO Astrophysics Symp., Growing Black Holes: Accretion in a Cosmological Context. Springer, Berline, p. 290
Tanaka Y., Boller T., Gallo L., Keil R., Ueda Y., 2004, PASJ, 56, L9
Titarchuk L., 1994, ApJ, 434, 570
Turner T. J., Pounds K. A., 1988, MNRAS, 232, 463
Zheng W. et al., 2001, ApJ, 562, 152
Życki P. T., Done C., Smith D. A., 1999, MNRAS, 309, 561

This paper has been typeset from a TEX/LATEX file prepared by the author.